nature nanotechnology

ARTICLES

PUBLISHED ONLINE: 27 OCTOBER 2013 | DOI: 10.1038/NNANO.2013.210

Nucleation, stability and current-induced motion of isolated magnetic skyrmions in nanostructures

J. Sampaio[1], V. Cros[1]*, S. Rohart[2], A. Thiaville[2] and A. Fert[1]

Magnetic skyrmions are topologically stable spin configurations, which usually originate from chiral interactions known as Dzyaloshinskii–Moriya interactions. Skyrmion lattices were initially observed in bulk non-centrosymmetric crystals, but have more recently been noted in ultrathin films, where their existence is explained by interfacial Dzyaloshinskii–Moriya interactions induced by the proximity to an adjacent layer with strong spin–orbit coupling. Skyrmions are promising candidates as information carriers for future information-processing devices due to their small size (down to a few nanometres) and to the very small current densities needed to displace skyrmion lattices. However, any practical application will probably require the creation, manipulation and detection of isolated skyrmions in magnetic thin-film nanostructures. Here, we demonstrate by numerical investigations that an isolated skyrmion can be a stable configuration in a nanostructure, can be locally nucleated by injection of spin-polarized current, and can be displaced by current-induced spin torques, even in the presence of large defects.

Information coding by a magnetic state is today the basis of the most massive information storage[1]. Magnetic skyrmions[2–4] are particle-like magnetic configurations as small as ~1 nm that are easily moved by small electrical currents[5–7], and provide a route to novel approaches to ultra-dense information storage, as well as to several types of purely solid-state spin-based information-processing devices[7,8]. For example, the concept of racetrack memory[9], in which a train of up and down magnetic domains is moved electrically along a magnetic track, could be extended to ultrahigh-density information-storage devices based on the manipulation of skyrmions in nanotracks[7,8].

Magnetic skyrmions[10] are chiral spin configurations that can be found either in magnetic materials with a non-centrosymmetric lattice or in magnetic ultrathin films in which the inversion symmetry is broken by the presence of non-equivalent interfaces. Skyrmion states are generally explained by the existence of Dzyaloshinskii–Moriya interactions[11–13] (DMIs) in systems lacking inversion symmetry. Because of their topological nature, the magnetic skyrmions are protected and consequently relatively stable, similarly to the other skyrmionic configurations first predicted in elementary particle physics[14] and later found in other fields of physics such as liquid crystals[15] or Bose–Einstein condensates[16].

Extended lattices of magnetic skyrmions were first observed in bulk non-centrosymmetric magnetic materials such as MnSi, (FeCo)Si or FeGe[2,3,17,18]. These skyrmion lattices can be moved by very small electrical currents[6] ($j_c \approx 1 \times 10^2$ A cm^{-2}) and simulations have indeed shown that, in comparison with the current-induced motion of domain walls, the flexibility of skyrmion lattices allows them to be far less hindered by defects[6].

In magnetic thin films, following the observation of several types of chiral spin configuration induced by interface DMIs[19,20], skyrmion lattices of extremely small size (nanometre range) have been observed by spin-polarized scanning tunnelling microscopy (STM) at zero field in one monolayer of Fe grown on Ir(111), and have been explained by the very large DMIs predicted for the Ir/Fe interface[4].

Here, we focus on simulations of isolated skyrmions or chains of skyrmions in nanostructured perpendicularly magnetized films and will not consider skyrmion lattices. The possible existence of isolated skyrmions generated by DMIs has already been predicted by Kiselev and colleagues[8]. We consider ultrathin magnetic films with an interface with a metal of large spin–orbit coupling and the following DMI between atomic spins $\mathbf{S}_1$ and $\mathbf{S}_2$ at the interface

$$\mathbf{H}_{DM} = -\mathbf{D}_{12}(\mathbf{S}_1 \times \mathbf{S}_2) \quad (1)$$

where $\mathbf{D}_{12}$ is the Dzyaloshinskii-Moriya (DM) vector. Such interface-induced DMIs had been predicted[21] from a three-site indirect exchange mechanism[22] coupling two atomic spins with a neighbour atom with large spin–orbit coupling. Their DM vector $\mathbf{D}_{12}$ is perpendicular to the unit vector joining $\mathbf{S}_1$ and $\mathbf{S}_2$ and is in the interface plane, which leads to hedgehog skyrmions instead of the vortex-like skyrmions generally observed with the bulk-like form of DMI[23] (we have verified that the main features of our results are valid for both types of skyrmion). A general advantage of skyrmions in thin films is that several parameters can be adjusted experimentally, such as the magnetic anisotropy K, modifiable for example by ion irradiation[24], or the DMI strength, which can be diluted by increasing the film thickness.

We performed micromagnetic simulations using the OOMMF code[25] (including the DMI[26]) for the following purposes: (1) to study the conditions for achieving stability of individual skyrmions in nanostructures at $T = 0$ K, (2) to test concepts for the creation or annihilation of isolated skyrmions, and (3) to investigate the spin transfer-induced motion of skyrmions in magnetic tracks with and without pinning by defects. Our simulations were performed with the form of DMI expressed by equation (2), the current-induced torques given by equations (3) to (6) and the parameters (A, K and α, respectively stiffness, perpendicular anisotropy and damping coefficients) corresponding to perpendicularly magnetized Co layers on Pt (listed in the Methods). Dipolar interactions were taken into account, but we found them to have negligible influence. For the DM parameter D (equation (2)), we considered values in large intervals around the one experimentally known[4] so that our

[1]Unité Mixte de Physique CNRS/Thales and Université Paris Sud, Palaiseau, France, [2]Laboratoire de Physique des Solides, Université Paris Sud, CNRS, Orsay, France. *e-mail: vincent.cros@thalesgroup.com

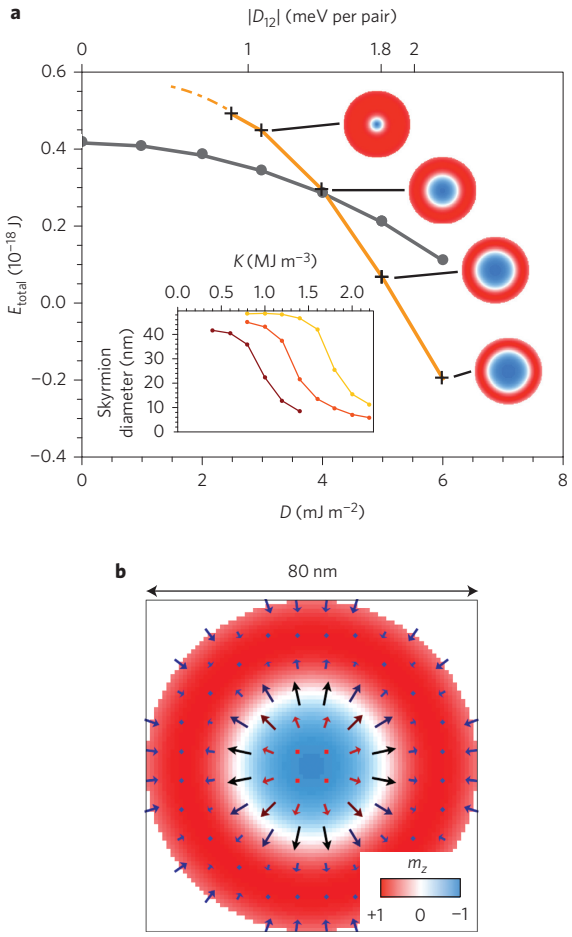

Figure 1 | Isolated skyrmion in a nanodisk (diameter, 80 nm). a, Total micromagnetic energy (including the DMI, exchange, dipolar and anisotropy energies) for an isolated skyrmion (yellow line and crosses) and FM states (grey line and circles) as a function of DM parameter D. The top horizontal axis shows the value of $|D_{12}|$ per pair of spins at the interface that corresponds to the value of D for a 0.4-nm-thick cobalt layer at the bottom scale. Note that 1.8 meV per pair is the value of $|D_{12}|$ found for the Fe/Ir(111) interface. Below $D = 2.2$ mJ m^{-2}, the skyrmion state is only stable with a smaller simulation cell (dashed yellow line). The magnetization m_z of the skyrmions for four values of D is shown. Inset: variation with anisotropy of the skyrmion diameter for different values of D (4, 5 and 6 mJ m^{-2} in brown, orange and yellow lines, respectively). **b**, Magnetization distribution in the skyrmion state for $D = 4$ mJ m^{-2}. Arrows represent the in-plane component. The colour scale for **a** and **b** is shown in the inset of **b**.

results could be applied to a large set of possible experimental systems with different interfaces and different thicknesses (Supplementary Section S1).

Stability of isolated skyrmions in nanodisks

We numerically calculated the relaxed micromagnetic state of 80-nm-wide nanodisks in zero field for different values of the DM parameter D and different initial magnetic configurations (see Methods). An example of our results for the variation of the total energy with D (including the DMI, the Heisenberg exchange interaction, dipolar interactions, as well as the magnetic anisotropy) is shown in Fig. 1a. Our central value of D (4 mJ m^{-2}) corresponds approximately to the experimental value for one monolayer of Fe on Ir(111), $|\mathbf{D}_{12}| = 1.8$ meV per atom pair[4], divided by two in order to take into account the dilution of the interface DMI in our 0.4-nm-thick layers.

We first consider the results of Fig. 1a with an initial uniform perpendicular magnetization along $+z$. Up to $D \approx 6$ mJ m^{-2}, we find that the relaxed stable state is still a quasi-uniform out-of-plane ferromagnetic state (FM). At higher D, the FM state is no longer stable and the system relaxes to a multidomain state with domain walls of a given chirality[20]. The decrease in the energy of the FM state with D in Fig. 1a is due to lowering of the DMI energy by an inward tilt of the spins at the edges[27].

In a second series of simulations, the initial state is skyrmion-like. For $D < 2.5$ mJ m^{-2}, the relaxed state is not a skyrmion but the FM state. For D in the range 2.5–6 mJ m^{-2}, the relaxed state is a skyrmion. This regime with a bistable system is the most interesting for applications: both the FM and single skyrmion states can be stabilized, the energy being smaller for the skyrmion above $D^* = 4$ mJ m^{-2} (for this disk diameter) and larger below D^* (D^* decreases from 5.6 to 3.8 mJ m^{-2} when the disk increases from 40 nm to infinity). For $D > 7$ mJ m^{-2}, the state with a single skyrmion becomes unstable and relaxes to a multiple-domain state.

As shown in Fig. 1a, the skyrmion size, defined as the diameter of the line $m_z = 0$, increases with D, in contrast to what is expected for skyrmion lattices in unbounded films, where the lattice period is proportional to A/D (ref. 7). In both systems, increasing D tends to increase the quantity of twisted spin pairs. In a skyrmion lattice where the density of skyrmions is a free parameter, an increase in D leads to the creation of more skyrmions of smaller size[8]. In contrast, with a single skyrmion (or any fixed number of skyrmions), the skyrmion spreads into a larger part of the disk (the skyrmion diameter depends on the dot diameter too; Supplementary Fig. S1A) and its size increases when D increases with respect to A and K. Finally we emphasize that, in confined structures with a fixed number of skyrmions, the skyrmion size can be reduced by increasing the anisotropy (inset of Fig. 1a).

We thus demonstrate that stable or metastable isolated skyrmions can be obtained in dots with realistic values of the DMI, exchange and anisotropy parameters. In Supplementary Section S1 (Supplementary Fig. S2), we show how the existence of the bistability region is robust against the variation of various parameters.

Nucleation of skyrmions by spin transfer torque

We propose a way to create isolated skyrmions in nanostructures of thin magnetic films. Such a process necessarily involves overcoming the topological stability barrier. Recently, solutions based on the use of local stray fields from a magnetic tip have been described[28,29]. Here, we investigate the option of creating a skyrmion by local injection of a spin-polarized current.

To investigate this nucleation mechanism, we performed micromagnetic simulations on the device geometry as described in Fig. 2 and composed of an 80 nm magnetic disk with a 40 nm inner disk for the injection of a current of spin polarization $P = 0.4$ along $-z$. We start with an initial FM state ($m = +\mathbf{e_z}$, that is, red dot) and apply a 2-ns-long current pulse. At low current density, as shown in Fig. 2a for $J = 1 \times 10^8$ A cm^{-2}, the initial FM configuration subsists. Above a threshold value J_{th} ($\sim 2 \times 10^8$ A cm^{-2} for our parameters) and at small values of D (2 and 3 mJ m^{-2} in Fig. 2), the magnetization is reversed (blue dot). For an intermediate D value (4 mJ m^{-2}), a multidomain state (separated by Dzyaloshinskii domain walls[30]) is the more stable final state. The most interesting result is the nucleation of a single skyrmion found for $D \geq 5$ mJ m^{-2} with a 2 ns current pulse of density $\geq 2 \times 10^8$ A cm^{-2}. Interestingly, the threshold current for nucleation can be significantly reduced by using magnetic materials with smaller α values than the one for Co ($\alpha = 0.3$) we used in these simulations. For example, if we take $\alpha = 0.015$, recently measured in perpendicularly magnetized CoFeB films[31], nucleation currents as small as 0.5×10^8 A cm^{-2} are found for $D = 3$ mJ m^{-2} (Fig. 2c). This current can be further reduced by applying a field along $-z$ to

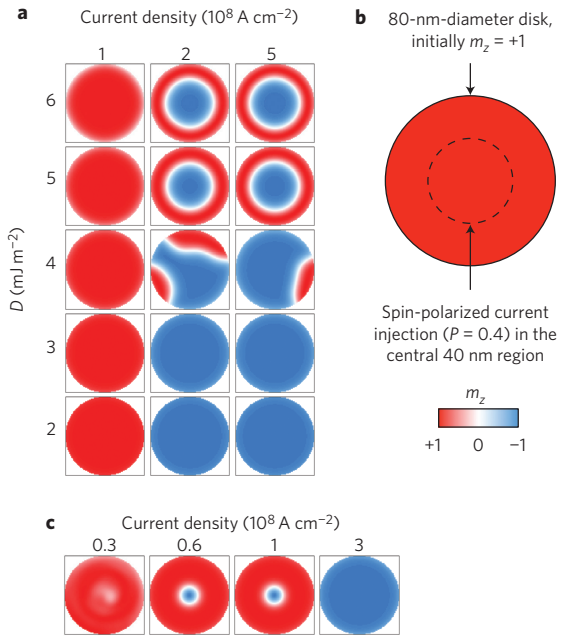

Figure 2 | Injection of skyrmions in a nanodisk. a, Magnetization in 80-nm nanodisks of different DM parameter D after injecting spin-polarized currents ($P = 0.4$) of different densities for 2 ns. The initial state at $t = 0$ was quasi-uniformly magnetized along $+z$ (red). **b**, Scheme of the injection device, showing the central region into which the polarized current is injected. **c**, As in **a**, but for optimized conditions (smaller current threshold and sizes), $\alpha = 0.015$ (the value of CoFeB films[41]), $D = 3$ mJ m^{-2}, external $H_z = -50$ mT and injection disk diameter of 20 nm. The colour scale for **a**–**c** is shown in **b**.

lower the energy barrier for magnetization reversal (or, equivalently, by lowering the perpendicular anisotropy coefficient). In these conditions, it becomes possible to create skyrmions with relatively small D similar to those needed in the bistability region.

The nucleation mechanism revealed by the simulations is rather complex (Supplementary Section S2; successive stages are provided in Supplementary Fig. S3). Usually, we first observe a reversed magnetization region[29] that develops in the region under the injection contact. The skyrmion number S (defined as $S = \frac{1}{4\pi}\int \mathbf{m} \cdot \left((\partial\mathbf{m}/\partial x) \times (\partial\mathbf{m}/\partial y)\right) dx dy$, where $\mathbf{m}$ is the normalized magnetization) of this magnetic configuration is ~ 0 (S is not exactly zero due to the contribution from the tilted spins at the edges[27]), thus being topologically identical to the initial uniform state. This situation is similar to that of a hard bubble surrounded by a pseudo-domain wall composed of two parts with opposite chiralities separated by Bloch lines (Supplementary Fig. S3). Then, in the mixed-chirality pseudo-wall surrounding the reversed region, the part with chirality favoured by the DMI spreads out continuously and compresses the other part into a small region inside the wall where a large positive DMI energy density is found (note that a similar phenomenon has been obtained in bubble materials by the impact of stray fields[32]). Eventually, the small defect-like region, by a process comparable to a Bloch point injection and film crossing in thicker magnetic systems, reverses and the skyrmion number changes to a value corresponding to a magnetic skyrmion ($S \approx 1$; again, the contribution from the tilted spins on the edge of the disk is responsible for a small reduction of S). Finally the skyrmion stabilizes its motion and becomes perfectly centred when the current pulse ends. Such a nucleation mechanism of an isolated skyrmion that relies on the concentration of energy in a singular defect cannot be described, in principle, micromagnetically (as it should require performing non-feasible simulations with zero mesh size). However, it has been shown that, in the case of a vortex core reversal occurring through the formation and propagation of a Bloch point[33,34], even if the mesh is finite in micromagnetic simulations, the Bloch point itself (of atomic size) sits between the mesh points, which allows any divergence to be avoided. Moreover, in a real sample, the mesh size cannot be smaller than the atomic spacing, and the presence of defects, or thermal fluctuations, requires an equivalent mesh that is much larger. A similar mechanism controlled by the existence of a singular magnetic defect has been recently proposed[35] to explain the destruction of a skyrmion lattice in a chiral $Fe_{1-x}Co_xSi$ magnet.

Finally, during the submission of our article, the possibility of writing and deleting individual skyrmions in experiments using a spin-polarized current has been reported in a non-structured ultrathin magnetic film submitted to an external applied field that helps to tune the energy landscape[36]. This experimental demonstration makes us even more confident that the future of information storage might be based on skyrmion configuration.

Current-induced motion of skyrmions in nanotracks

Skyrmions can be moved at low current densities by spin transfer torques[6,7,37,38]. According to the simulations by Iwasaki and colleagues[6] on skyrmion lattices, this easy motion is mainly due to very weak pinning by defects. Here, we demonstrate that spin transfer torques can also be used to move individual skyrmions or chains of skyrmions in nanotracks (with typical cross-section of 40×0.4 nm^2).

We studied the current-induced motion of metastable skyrmions existing in long tracks for D smaller than the upper bound $D^* = 3.8$ mJ m^{-2} found for a disk of infinite radius. Our simulations were performed with circular skyrmions for $D = 3$ mJ m^{-2}. Note that, for $D > D^*$, the skyrmions adopt an elongated shape in the direction of the nanotrack.

Considering, first, spin-polarized currents injected in-plane, we introduced adiabatic and non-adiabatic spin torques[39] (equations (3) and (4)) with different values of the non-adiabatic parameter β (keeping the Gilbert damping of Co/Pt, $\alpha = 0.3$). As shown in Fig. 3b, during an initial transient regime (<1 ns) the skyrmion has a longitudinal velocity (x-direction) and a transverse velocity in the $+y$-direction for $\beta > \alpha$ and the $-y$ direction for $\beta < \alpha$. The transverse motion along y stops at some distance from the edge because of the repulsive interaction due to the tilting of magnetization on the track edges[27] induced by DMI (see the description according to the Thiele equation in Supplementary Section S4). The motion is then longitudinal with a steady velocity approximately equal to $u\beta/\alpha$, where u is proportional to the current density j (ref. 40). For very large current densities, typically 100 MA cm^{-2}, the skyrmion can reach the edge and is expelled (ends of the curves in Fig. 3a). Particular situations correspond to $\beta = \alpha$ (no transverse motion, longitudinal motion along the central line) and $\beta = 0$ (no steady motion).

The confinement in the track introduces important differences with respect to the motion of free skyrmion lattices, in which the existence of a steady transverse velocity introduces an additional force in the Thiele equation and leads to a longitudinal velocity $v_{\parallel} = u$, independently of the values of both β and α (ref. 7).

The second situation we consider is the vertical injection of a spin current polarized along $\mathbf{e_Y}$, which can be obtained either by injection from a magnetic tunnel junction or by the spin Hall effect[40] (see Methods). For domain wall motion, this situation optimizes the action of the spin torque because the driving torque is directly the larger Slonczewski in-plane torque and not the smaller field-like out-of-plane torque[41,42]. This situation results in skyrmions with much larger velocities than with in-plane ones (Fig. 3a). After a short transient regime, the skyrmion moves at a constant velocity along the track direction (Fig. 3b). The velocity is found to be inversely proportional to the damping parameter α

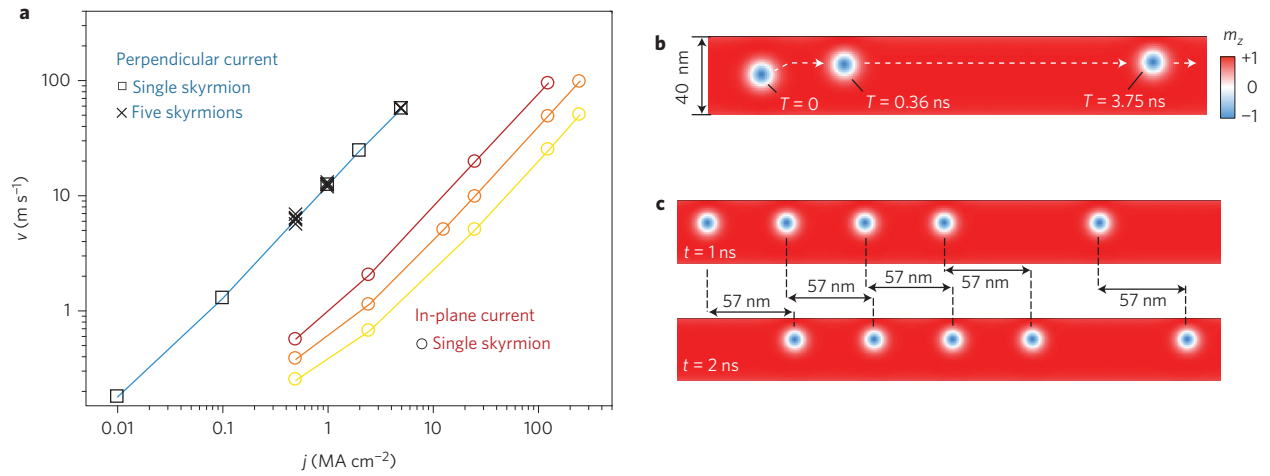

Figure 3 | Current-induced motion of skyrmions in a nanotrack. a, Skyrmion velocity v as a function of current density j for in-plane currents with different values of the non-adiabaticity parameter β (0.15, 0.30 and 0.60 in yellow, orange and brown lines and circles, respectively) and for vertical currents (blue line, squares for isolated skyrmion, crosses for the chain in **c**). The slight deviation from linearity for $j < 1$ MA cm^{-2} is probably due to an insufficient simulation time in a situation with very slow propagation velocity. **b**, Trajectory of a single skyrmion (white dotted line) driven by a vertical current ($j = 5$ MA cm^{-2}, $v = 57$ m s^{-1}). **c**, Chain of five skyrmions with two different spacings driven by a vertical current ($j = 5$ MA cm^{-2}) at $t = 1$ ns and 2 ns. For all simulations, we used $D = 3$ mJ m^{-2} and current polarization $P = 0.4$. The colour scale for **b** and **c** is shown in **b**.

(in agreement with the analytical expression of the velocity derived from the Thiele equation[43]), so, as for skyrmion nucleation, the choice of films with smaller α values than that of cobalt ($\alpha = 0.3$) will lead to larger velocities. We have checked that opposite currents, polarizations or D change the motion direction. In contrast to the current-induced motion of domain walls, there is no intrinsic pinning, the skyrmion velocity increasing linearly with the current density.

We conclude that vertical current injection can very efficiently move skyrmions in a track at speeds of ~10 m s^{-1} per MA cm^{-2}. In fact, there is a definite analogy between the motion of skyrmions by vertical currents and the motion of DMI-induced Néel domain walls by the spin Hall effect described by Thiaville and colleagues[30] and illustrated by recent experimental results with very large domain wall velocities in bilayers such as Pt/Co[44–46].

Chain of skyrmions in nanotracks

A very dense encoding of information could be achieved by using a chain of skyrmions in a nanotrack. To provide a proof of feasibility, we performed simulations of the motion induced by a vertical current for a chain of five skyrmions, the first four 50 nm apart (centre-to-centre) and the last 100 nm apart. It turns out that (as shown in Fig. 3c) all the skyrmions move along the same trajectories as single skyrmions with the same velocities (compare crosses and squares in Fig. 3a). An important feature is the conservation of the initial spacing.

Our results are very appealing from the perspective of using chains of skyrmions instead of chains of domains in shift register 'racetrack' memories[9]. The main advantages of skyrmions are related to their small size and their facile current-induced motion by, for example, the spin Hall effect in the metal layer with large spin–orbit coupling beneath the magnetic track. Moreover, their topological protection is expected to drastically reduce the influence of defects. To study this issue, we placed some repulsive triangular notches of stronger perpendicular anisotropy ($K = 1.2$ MJ m^{-3} instead of 0.8 MJ m^{-3}) and variable sizes (insets of Fig. 4) into the skyrmion trajectory. Depending on the current density, the skyrmion stops when it runs into the notch (lower inset and filled circles and orange shading, Fig. 4) or, at larger current density, moves around the notch and continues on its initial trajectory with its initial velocity (upper inset and open circles and blue shading, Fig. 4). The current density preventing the pinning is in the MA cm^{-2} range for notches up to 20 nm (half the track width) and decreases to ~0.07 MA cm^{-2} for notches of a few nanometres. Note that these depinning densities are slightly larger than those derived from experiments[37] or simulations[7] with skyrmion lattices, but still definitely smaller than those for domain walls with similar defects.

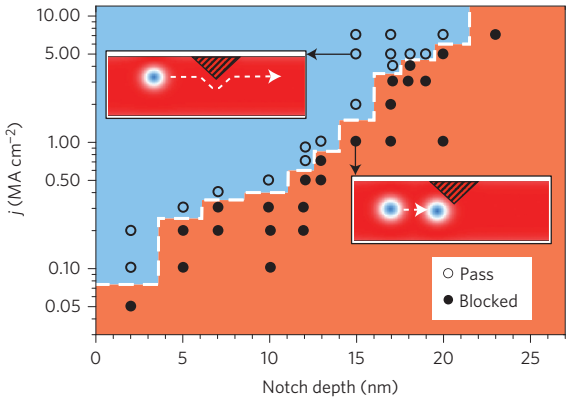

Figure 4 | Pinning of the current-induced motion of skyrmions by defects in a 40-nm-wide nanotrack. The defect (notch) is a triangular region of higher perpendicular anisotropy ($K = 1.2$ MJ m^{-3} instead of 0.8 MJ m^{-3} for the rest of the track), and the motion has been simulated for different notch depths (horizontal axis) and different spin-polarized current densities j (vertical axis, spin polarization $P = 0.4$). Open and filled circles indicate couples of depth and current for which the skyrmion passes the notch and remains pinned, respectively. The boundary between the blue and brown zones is an approximate indication of the evolution of the depinning current with notch depth. Top inset: trajectory of a skyrmion (white dotted line) around a 15-nm-deep notch driven by a current with $j = 5$ MA cm^{-2}. Bottom inset: pinning at the same notch at $j = 1$ MA cm^{-2}. The colour code represents m_z (red for +1, white for 0 and blue for −1).

Perspectives

Our objective was to assess realistically the possibility of developing devices based on the nucleation, manipulation and detection of

skyrmions or groups of skyrmions in nanostructured thin films. We performed our simulations with interface-induced DMIs in the range expected from recent experiments and *ab initio* calculations at interfaces between ferromagnetic and nonmagnetic 5*d* metals[4]. The stabilization of isolated skyrmions is not a breakthrough as it has already been predicted by analytical calculations[8], but the numerical simulations give more insight into the possible control of skyrmion size by playing with various parameters. An important part of our study is the mechanism for the nucleation of isolated skyrmions by the injection of vertical spin-polarized current pulses. With the relatively large damping parameter taken for Co/Pt films ($\alpha = 0.3$), the nucleation requires relatively large current densities ($\sim 1 \times 10^8$ A cm^{-2}), but we have shown that this density can be reduced significantly in magnetic films of smaller α, smaller perpendicular anisotropy or by applying a magnetic field. The detection can be achieved by magnetoresistive effects. Finally, we investigated the current-induced motion of a skyrmion or a train of skyrmions in a nanotrack. We found that the most efficient mechanism to obtain high velocities is the vertical injection of a spin-polarized current from a magnetic tunnel junction or by the spin Hall effect. As the skyrmions also appear to be very weakly pinned by defects, their current-induced motion is very promising for obtaining large information flows with small energy consumption. We hope that our simulations can be a guide for the development of skyrmion-based devices.

Methods

We consider a 0.4-nm-thick cobalt film with perpendicular magnetic anisotropy on a substrate inducing DMIs. In a continuous magnetization model, the DMI can be expressed as[30]

$$\varepsilon_{\mathrm{DM}} = D\left(m_z \frac{\partial m_x}{\partial x} - m_x \frac{\partial m_z}{\partial x} + m_z \frac{\partial m_y}{\partial y} - m_y \frac{\partial m_z}{\partial y}\right) \quad (2)$$

where m_x, m_y, m_z are the components of the normalized magnetization $\mathbf{m} = \mathbf{M}/M_S$. This corresponds to a DM vector $\mathbf{D_{12}}$ in equation (1) perpendicular to the unit vector joining the two spins in the interface plane. D is an area unit energy density related to the strength of $\mathbf{D_{12}}$ with a $1/at$ proportional factor (where a is the atomic lattice constant and t is film thickness). For the case of a face-centred cubic lattice with (111) perpendicular to the film, the continuous DMI constant is $D = |D_{12}|\sqrt{3}/at$.

We performed finite-element micromagnetic simulations using the OOMMF code modified to include the DMI. The discretization cell δx was 1 nm (0.2 nm for a skyrmion below 6 nm). The saturation magnetization $M_S = 580$ kA m^{-1} was measured by superconducting quantum interference device (SQUID) magnetometry in an as-deposited film of 0.4 nm of cobalt on platinum grown by sputtering deposition and capped by an alumina layer. The exchange stiffness ($A = 15$ pJ m^{-1}), perpendicular magnetocrystalline anisotropy ($K_u = 0.8$ MJ m^{-3}, which results in an effective anisotropy of $K_{\mathrm{eff}} = 0.6$ MJ m^{-3}) and Gilbert damping ($\alpha = 0.3$) come from experimental results for the Pt/Co system[47]. Finally, D was taken to be between 0 and 9 mJ m^{-2} ($\sim$5 mJ m^{-2} corresponds approximately to the value 1.8 meV for spin pairs found for iron monolayers on iridium[5]). Finally, we defined the skyrmion diameter as the diameter of the circle of $m_Z = 0$.

For simulations of the spin transfer torque associated with the current in-plane (CIP) injection geometry, the two following torques were added to the Ladau-Lifschitz-Gilbert equation:

$$\tau_{\mathrm{adiab.}} = u\mathbf{m} \times \left(\frac{\partial \mathbf{m}}{\partial x} \times \mathbf{m}\right) \quad (3)$$

$$\tau_{\mathrm{non\_adiab.}} = \beta u\left(\mathbf{m} \times \frac{\partial \mathbf{m}}{\partial x}\right) \quad (4)$$

where $u = \gamma(\hbar jP/2eM_S)$, $+x$ is the direction of the electron velocity, γ is the gyromagnetic ratio, M_S is the saturation magnetization, j is the current density, P is the spin polarization, and β is the non-adiabaticity factor[39].

For simulations with vertical spin currents, the in-plane and out-of-plane torques are written as[40]

$$\tau_{\mathrm{IP}} = \frac{u}{t}\mathbf{m} \times (\mathbf{m}_{\mathrm{p}} \times \mathbf{m}) \quad (5)$$

$$\tau_{\mathrm{OOP}} = -\xi\frac{u}{t}(\mathbf{m} \times \mathbf{m}_{\mathrm{p}}) \quad (6)$$

where t is the film thickness and ξ is the amplitude of the out-of-plane torque relative to the in-plane one and $\mathbf{m}_{\mathrm{p}}$ is the current polarization vector. The only case for which we find a steady motion of the skyrmions is when $\mathbf{m}_{\mathrm{p}}$ is oriented along y direction i.e. in the film plane and transverse to the long side of the track. This configuration of the polarization vector can be obtained by Spin Hall effect for example. Note that, for films thinner than the absorption length of spin transfer (precession length in the exchange field), the incomplete spin transfer of the injected spin current can be taken into account by a renormalized spin polarization P. The Oersted field was also included.

For the skyrmion state, the initial configuration could be either similar to a 'hedgehog' skyrmion (radial $\mathbf{m}_{\mathrm{plane}}$) or to a vortex-like one, and two different chiralities (clockwise or anticlockwise) could also be chosen. As already mentioned, our simulations show that only the hedgehog skyrmion was stable in our thin-film system, and the vortex skyrmion tended to relax to either the FM state or the hedgehog skyrmion. Note that the chiralities of skyrmions (as defined by the sense of rotation of the magnetization along the skyrmion diameter) is imposed by the sign of the DMI, which makes the hedgehog skyrmions of a different nature to magnetic bubbles generated by dipole–dipole interactions. Indeed, if we started the simulations with a skyrmion of opposite chirality, it consistently reversed to an FM or multidomain state.

Received 7 June 2013; accepted 16 September 2013; published online 27 October 2013

References

1. Chappert, C., Fert, A. & Van Dau, F. N. The emergence of spin electronics in data storage. *Nature Mater.* **6,** 813–823 (2007).
2. Muhlbauer, S. *et al.* Skyrmion lattice in a chiral magnet. *Science* **323,** 915–919 (2009).
3. Yu, X. Z. *et al.* Real-space observation of a two-dimensional skyrmion crystal. *Nature* **465,** 901–904 (2010).
4. Heinze, S. *et al.* Spontaneous atomic-scale magnetic skyrmion lattice in two dimensions. *Nature Phys.* **7,** 713–718 (2011)
5. Jonietz, F. *et al.* Spin transfer torques in MnSi at ultralow current densities. *Science* **330,** 1648–1651 (2010).
6. Iwasaki, J., Mochizuki, M. & Nagaosa, N. Universal current–velocity relation of skyrmion motion in chiral magnets. *Nature Commun.* **4,** 1463 (2013).
7. Fert, A., Cros, V. & Sampaio, J. Skyrmions on the track. *Nature Nanotech.* **8,** 152–156 (2013).
8. Kiselev, N. S., Bogdanov, A. N., Schäfer, R. & Rößler, U. K. Chiral skyrmions in thin magnetic films: new objects for magnetic storage technologies? *J. Phys. D* **44,** 392001 (2011).
9. Parkin, S. S. P., Hayashi, M. & Thomas, L. Magnetic domain-wall racetrack memory. *Science* **320,** 190–194 (2008).
10. Rössler, U. K., Bogdanov, A. N. & Pfleiderer, C. Spontaneous skyrmion ground states in magnetic metals. *Nature* **442,** 797–801 (2006).
11. Dzyaloshinskii, I. A thermodynamic theory of 'weak' ferromagnetism of antiferromagnetics. *J. Phys. Chem. Solids* **4,** 241–255 (1958).
12. Moriya, T. Anisotropic superexchange interaction and weak ferromagnetism. *Phys. Rev.* **120,** 91–98 (1960).
13. Crépieux, A. & Lacroix, C. Dzyaloshinskii–Moriya interactions induced by symmetry breaking at a surface. *J. Magn. Magn. Mater.* **182,** 341–349 (1998).
14. Skyrme, T. H. R. A unified field theory of mesons and baryons. *Nucl. Phys.* **31,** 556–569 (1962).
15. Wright, D. C. & Mermin, N. D. Crystalline liquids the blue phases. *Rev. Mod. Phys.* **61,** 385–432 (1989).
16. Al'Khawaja, U. & Stoof, H. T. C. Skyrmions in a ferromagnetic Bose–Einstein condensate. *Nature* **411,** 918–920 (2001).
17. Yu, X. Z. *et al.* Skyrmion flow near room temperature and ultralow current density. *Nature Commun.* **3,** 988 (2012).
18. Huang, S. X. & Chien, C. L. Extended skyrmion phase in FeGe (111) thin films. *Phys. Rev. Lett.* **108,** 267201 (2012).
19. Ferriani, P. *et al* Atomic scale spin spiral with a unique rotational sense: Mn monolyer on W(001). *Phys. Rev. Lett.* **101,** 027201 (2008).
20. Heide, M., Bihlmayer, G. & Blügel, S. Dzyaloshinskii–Moriya interaction accounting for the orientation of magnetic domains in ultrathin films: Fe/W (110). *Phys. Rev. B* **78,** 140403 (2008).
21. Fert, A. Magnetic and transport properties of metallic multilayers. *Metallic Multilayers* **59–60,** 439 (1990).
22. Fert, A. & Levy, P. M. Role of anisotropic exchange interactions in determining the properties of spin-glasses. *Phys. Rev. Lett.* **44,** 1538–1541 (1980).
23. Sun, L. *et al.* Creating an artificial two-dimensional skyrmion crystal by nanopatterning. *Phys. Rev. Lett.* **110,** 167201 (2013).
24. Chappert, C. *et al.* Planar patterned magnetic media obtained by ion irradiation. *Science* **280,** 1919–1922 (1998).
25. Donahue, M. J. & Porter, D. OOMMF (NIST); http://math.nist.gov/oommf
26. http://www.lps.u-psud.fr/spip.php?article2252
27. Rohart, S. & Thiaville, A. Micromagnetism of ultrathin film nanostructures in the presence of Dzyaloshinskii–Moriya interactions. Preprint at http://arXiv.org/abs/1310.0666 (2013).

28. Kirakosyan, A. S. & Pokrovsky, V. L. From bubble to skyrmion: dynamic transformation mediated by a strong magnetic tip. *J. Magn. Magn. Mater.* **305,** 413–422 (2006).
29. Mohseni, S. M. *et al.* Spin torque-generated magnetic droplet solitons. *Science* **339,** 1295–1298 (2013).
30. Thiaville, A., Rohart, S., Jué, É., Cros, V. & Fert, A. Dynamics of Dzyaloshinskii domain walls in ultrathin magnetic films. *Europhys. Lett.* **100,** 57002 (2012).
31. Devolder, T. *et al.* Damping of $Co_xFe_{80-x}B_{20}$ ultrathin films with perpendicular magnetic anisotropy. *Appl. Phys. Lett.* **102,** 022407 (2013).
32. Moutafis, C., Komineas, S. & Bland, J. A. C. Dynamics and switching processes for magnetic bubbles in nanoelements. *Phys. Rev. B* **79,** 224429 (2009).
33. Nakatani, Y. & Hayashi, N. Computer simulation of annihilation process of vertical Bloch line pair. *IEEE Trans. Magn.* **29,** 2587–2589 (1993).
34. Thiaville, A., Garcia, J. M., Dittrich, R., Miltat, J. & Schrefl, T. Micromagnetic study of Bloch point mediated vortex core reversal. *Phys. Rev. B* **67,** 094410 (2003).
35. Milde, P. *et al.* Unwinding of a skyrmion lattice by magnetic monopoles. *Science* **340,** 1076–1080 (2013).
36. Romming, N. *et al.* Writing and deleting single magnetic skyrmions, *Science* **341,** 636–639 (2013).
37. Schulz, T. *et al.* Emergent electrodynamics of skyrmions in a chiral magnet. *Nature Phys.* **8,** 301–304 (2012).
38. Everschor, K. *et al.* Rotating skyrmion lattices by spin torques and field or temperature gradients. *Phys. Rev. B* **86,** 054432 (2012).
39. Thiaville, A., Nakatani, Y., Miltat, J. & Suzuki, Y. Micromagnetic understanding of current-driven domain wall motion in patterned nanowires. *Europhys. Lett.* **69,** 990–996 (2005).
40. Khvalkovskiy, A. V. *et al.* Matching domain-wall configuration and spin–orbit torques for efficient domain-wall motion. *Phys. Rev. B* **87,** 020402 (2013).
41. Khvalkovskiy, A. *et al.* High domain wall velocities due to spin currents perpendicular to the plane. *Phys. Rev. Lett.* **102,** 067206 (2009).
42. Chanthbouala, A. *et al.* Vertical-current-induced domain-wall motion in MgO-based magnetic tunnel junctions with low current densities. *Nature Phys.* **7,** 626–630 (2011).
43. Thiele, A. Steady state motion of magnetic domains. *Phys. Rev. Lett.* **30,** 230–233 (1973).
44. Miron, I. M. *et al.* Fast current-induced domain-wall motion controlled by the Rashba effect. *Nature Mater.* **10,** 419–423 (2011).
45. Emori, S. *et al.* Current-driven dynamics of chiral ferromagnetic domain walls. *Nature Mater.* **12,** 611–616 (2013).
46. Ryu, K. S. *et al.* Chiral spin torque at magnetic domain walls. *Nature Nanotech.* **8,** 527–533 (2013).
47. Metaxas, P. J. *et al.* Creep and flow regimes of magnetic domain-wall motion in ultrathin Pt/Co/Pt films with perpendicular anisotropy. *Phys. Rev. Lett.* **99,** 217208 (2007).

Acknowledgements

We thank N. Reyren, C. Luchaire-Moreau, J. M. George and J. V. Kim for discussions, C. Deranlot for material deposition, and N. Van Horne, K. Bouzehouane and R. Mattana for magnetic measurements.

Author contributions

V.C. and A.F. conceived and coordinated the project. J.S. performed the micromagnetic simulations. S.R. implemented the DMI in the OOMMF code. J.S., V.C., S.R, A.T. and A.F. interpreted the results. J.S, V.C. and A.F. prepared the manuscript. All authors commented on the manuscript.

Additional information

Supplementary information is available in the online version of the paper. Reprints and permissions information is available online at www.nature.com/reprints. Correspondence and requests for materials should be addressed to V.C.

Competing financial interests

The authors declare no competing financial interests.